UC Irvine

Title
In Situ TEM Study of the Degradation of PbSe Nanocrystals in Air

Permalink

Journal

ISSN

Authors
Peng, Xinxing
Abelson, Alex
Wang, Yu
et al.

Publication Date

DOI

Peer reviewed

In Situ TEM Study of the Degradation of PbSe Nanocrystals in Air

Xinxing Peng,[†,‡] Alex Abelson,[§] Yu Wang,[‡,⊥] Caroline Qian,[§] Junyi Shangguan,[‡,⊥] Qiubo Zhang,[‡] Lei Yu,[‡,⊥] Zu-Wei Yin,[†,‡] Wenjing Zheng,[‡,⊥] Karen C. Bustillo,[#] Xuyun Guo,[∥] Hong-Gang Liao,*[,†] Shi-Gang Sun,[†] Matt Law,[§] and Haimei Zheng*[,‡,⊥]

[†]State Key Lab of Physical Chemistry of Solid Surfaces, Collaborative Innovation Center of Chemistry for Energy Materials, College of Chemistry and Chemical Engineering, Xiamen University, Xiamen, 361005, P. R. China

[‡]Materials Science Division, Lawrence Berkeley National Laboratory, Berkeley, California 94720, United States

[§]Department of Chemical Engineering and Department of Chemistry, University of California, Irvine, Irvine, California 92697, United States

[#]National Center for Electron Microscopy, Molecular Foundry, Lawrence Berkeley National Laboratory, Berkeley, California 94720, United States

[⊥]Department of Materials Science and Engineering, University of California, Berkeley, Berkeley, California 94720, United States

[∥]Department of Applied Physics, The Hong Kong Polytechnic University, Hung Hom, Kowloon, Hong Kong, P. R. China

S *Supporting Information*

ABSTRACT: PbSe nanocrystals have attracted widespread attention due to a variety of potential applications. However, the practical utility of these nanocrystals has been hindered by their poor air stability, which induces undesired changes in the optical and electronic properties. An understanding of the degradation of PbSe nanocrystals when they are exposed to air is critical for improving the stability and enhancing their applications. Here, we use in situ transmission electron microscopy (TEM) with an environmental cell connected to air to study PbSe nanocrystal degradation triggered by air exposure. We have also conducted a series of complementary studies, including in situ environmental TEM study of PbSe nanocrystals exposed to pure oxygen and PbSe nanocrystals in

H_2O using a liquid cell, and ex situ experiments, such as O_2 plasma treatment and thermal heating of PbSe nanocrystals under different air exposure. Our in situ observations reveal that when PbSe nanocrystals are exposed to air (or oxygen) under electron beam irradiation, they experience a series of changes, including shape evolution of individual nanocrystals with the cuboid intermediates, coalescence between nanocrystals, and formation of PbSe thin films through drastic solid-state fusion. Further studies show that the PbSe thin films transform into an amorphous Pb rich phase or eventually pure Pb, which suggest that Se reacts with oxygen and can be evaporated under electron beam illumination. These various in situ and ex situ experimental results indicate that PbSe nanocrystal degradation in air is initiated by the dissociation and removal of ligands from the PbSe nanocrystal surface.
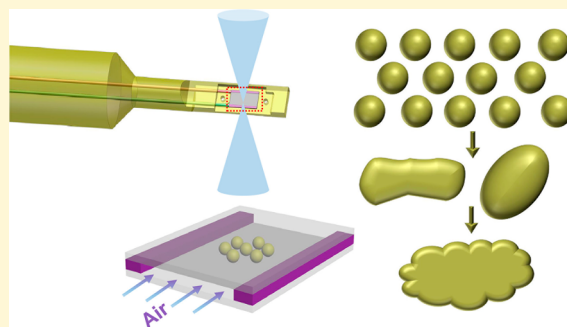
INTRODUCTION

Semiconductor nanocrystals continue to attract considerable attention because of their various applications in solar cells,[1] light-emitting diodes,[2] and field-effect transistors.[3] Monodisperse colloidal PbX (X = S, Se, Te) nanocrystals are ideal building blocks for fabricating mesoscale materials with emergent collective properties. For example, PbSe nanocrystals capped with oleate ligands can self-assemble into superlattices exhibiting excellent long-range ordering.[4−8] The nanocrystals in these assemblies can then be fused together along their (100) facets by controllably stripping the oleate ligands to yield epitaxially fused superlattices.[9,10] These epi-superlattices are now of interest because of the potential for band-like charge transport, the achievement of which would be a significant achievement in mesoscale materials science.

However, species such as oxygen and some solvents (e.g., H_2O) have been shown to eliminate the preference for (100) fusion and instead promote random necking.[11] The mechanisms by which air exposure and variations in ligand coverage impact nanocrystal fusion are not well understood.

Unlike bulk materials, nanocrystals are susceptible to large morphological changes with variations in surface chemistry due to their large surface-to-volume ratio.[12] One ubiquitous concern is the impact of oxygen exposure on the optical and electronic properties of air-sensitive nanocrystals. It has been shown that PbSe nanocrystals can rapidly oxidize to become a
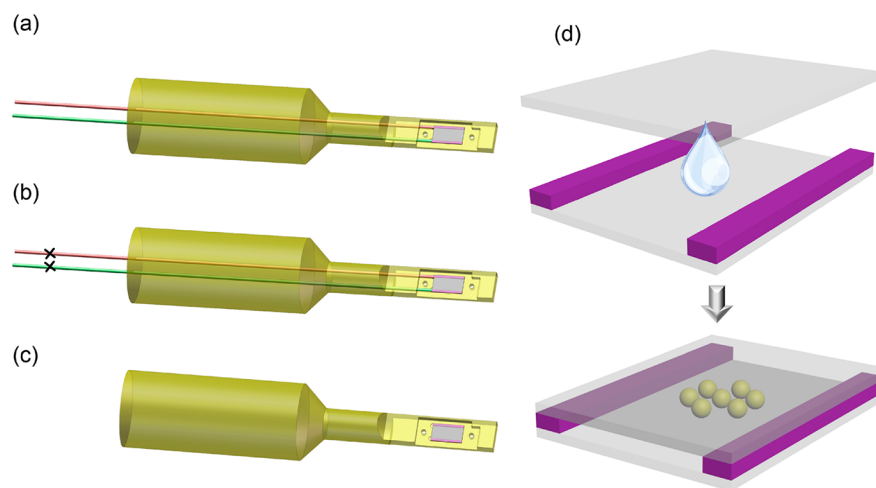
Figure 1. Schematic of the experimental setup for imaging of PbSe nanocrystals under different environmental conditions. (a) PbSe nanocrystals are fully exposed to air when they are in an environmental cell with the connecting tubes open. (b) PbSe nanocrystals are partially exposed to air when they are in an environmental cell with the tubes sealed with parafilm. Trace amount of air can diffuse through the parafilm into the tube. (c) PbSe nanocrystals are under vacuum environment when they are in a traditional single tilt holder. (d) Preparation of monolayer-thick of PbSe nanocrystal superlattices in an environmental cell by drop-casting the PbSe nanocrystal solution on the bottom chip and assembling it with the top chip. The bottom chip is patterned with a layer of silicon dioxide to create a flow tunnel.

more conductive p-type material under ambient conditions, causing serious issues for their use in devices.[3,13] Efforts have been made on the study of PbX (X = Cl, Br, I) nanocrystal surface chemistry. PbX nanocrystals adopt the rock-salt structure and are often terminated by a combination of (100), (110), and (111) facets.[14,15] The Pb atoms on polar (111) facets coordinate with ligands for charge balance, which reduces the surface energy and makes the polar facet more stable compared to the (100) and (110) facets with sparser ligand coverage.[4,16] Passivation of (100) facets with atomically thin PbX_2 (X = Cl, Br, I) adlayers has also improved the air stability of PbSe nanocrystals.[17] Additionally, optical and X-ray photoelectron spectroscopy studies of PbSe nanocrystal films have provided evidence that surface oxidation is the main degradation issue leading to significant changes in the electronic structure.[18,19] The chemisorption of oxygen on PbSe nanocrystals can lead to the growth of an oxide layer on the surface, on which complex oxidation chemistry and kinetics have been studied[20,21] and different metal oxides including PbO, SeO_2, and $PbSeO_3$ have been observed.[22−24] Many advanced methods have been developed to improve the ambient stability of PbX nanocrystals, including halogen treatment,[25] cation exchange,[26] precursor engineering,[27] surface coating,[28] and atomic layer deposition infilling.[29] For instance, passivation of PbSe nanocrystals through ion exchange leads to solar cells with >8% efficiency, maintaining at least 93% of their initial power conversion efficiency after being stored for 57 days.[26] Although the oxidation mechanism and protection techniques of PbSe nanocrystals have been widely studied, the physicochemical changes that plague nanocrystals are still not fully understood due to the lack of detailed information on the degradation pathways of nanocrystals upon exposure to air.

In situ environmental cell TEM provides unique capabilities for the direct observation of materials transformations during reactions in relevant gas[30,31] or liquid environments.[32] A variety of dynamic phenomena have been visualized with high spatial and temporal resolution using in situ TEM, including surface reconstruction,[33] nucleation, and growth of nanocryst-

als[34−38] and precipitation and dissolution at electrode−electrolyte interfaces.[39] Here, we use the environmental cell setup to study PbSe nanocrystal degradation by exposing them to static air. The effects of air exposure on the structural instability of PbSe nanocrystals are investigated through a set of in situ experiments with nanocrystals inside the cell fully exposed to air (tubes are open to air), partially exposed to air (tubes are sealed with parafilm), and in vacuum (using a conventional vacuum sample holder with no tubes) (Figure 1). The structural evolution of the PbSe nanocrystals under different degrees of air exposure with electron beam irradiation is captured in situ. We also conduct complementary experiments including in situ gas environmental TEM experiments by exposing PbSe nanocrystals to pure O_2 and PbSe nanocrystals in water and systematic ex situ studies of PbSe nanocrystals when exposed to O_2 plasma or after thermal heating in various environments, which provide important supplementary information on the degradation of PbSe nanocrystals.

■ EXPERIMENTAL SECTION

Chemicals. All commercially available chemicals were used without further purification. Lead(II) oxide (PbO, 99.9995%, Alfa Aesar), selenium shot (99.999%), oleic acid (OA, tech. grade, 90%), diphenylphosphine (DPP, 98%, Aldrich), trioctylphosphine (TOP, tech. grade, >97%, Strem Chemicals Inc.), 1-octadecene (ODE, 90%, Aldrich), hexane (anhydrous, ≥99%, Sigma-Aldrich), and ethyl alcohol (anhydrous, ≥99.5%, Sigma-Aldrich) were used in nanocrystals synthesis, purification, and washing.

Synthesis. PbSe nanocrystals were synthesized and purified using standard air-free techniques. In a typical synthesis, 1.50 g of PbO, 5.0 g of OA, and 10.0 g of ODE were added to a three-neck flask and thoroughly degassed under a dynamic vacuum of ∼50 mTorr at room temperature. The mixture was then heated under vacuum at 110 °C for 1.5 h to produce a dry solution of $Pb(OA)_2$. The solution was heated to 180 ± 3 °C under flowing argon, at which point 9.5 mL of a 1 M solution of TOP-Se containing 0.20 mL of DPP was rapidly injected to trigger the nucleation. After 105 ± 3 s, the reaction was quenched by immersion in a bath of liquid nitrogen, cooled to 35 °C, and diluted with 10 mL of anhydrous hexanes. Inside an N_2-filled glovebox (O_2 < 10 ppm), the nanocrystals were purified by three
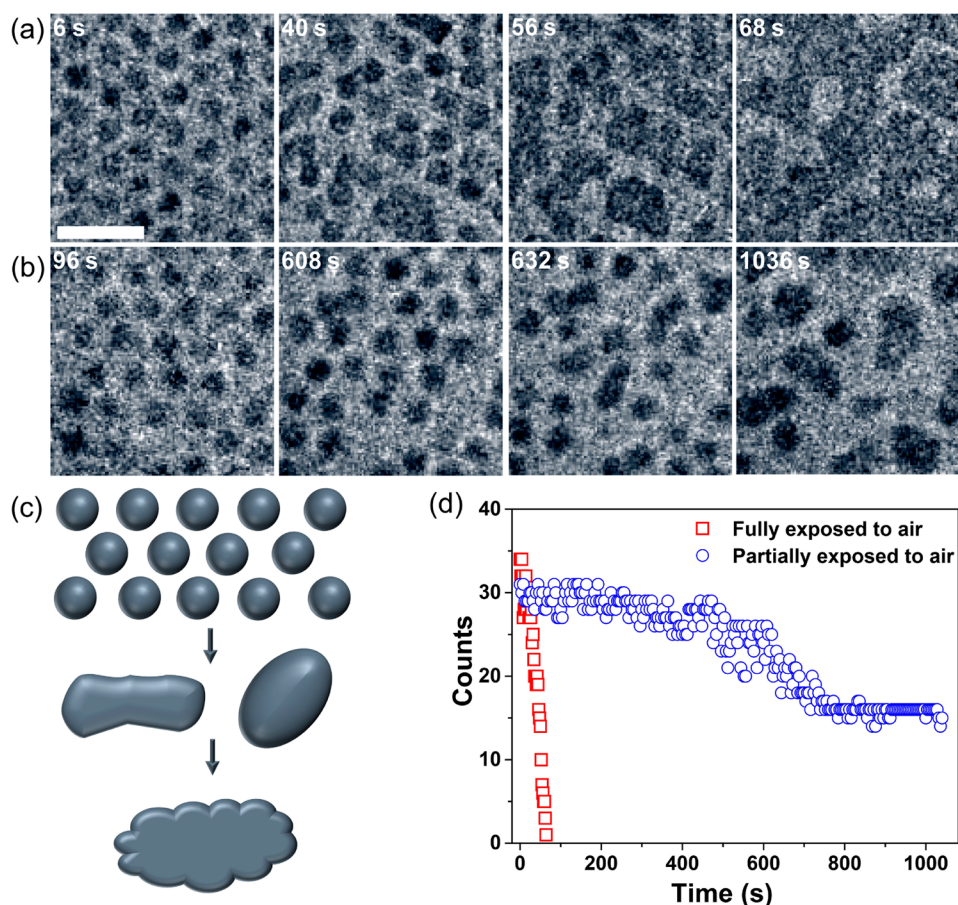
Figure 2. Morphology changes of PbSe nanocrystals under maximum or partial exposure to air. (a) Sequential TEM images showing the morphology changes of PbSe nanocrystals under maximum exposure to air and (b) partial exposure to air. (c) A schematic showing the trend of morphology evolution of PbSe nanocrystals when exposed to air. (d) The numbers of nanocrystals as a function of time corresponding to (a) and (b). Scale bar: 20 nm.

rounds of precipitation–redispersion with ethanol/hexane, dried completely, and stored as a powder.

In Situ and ex Situ TEM Study of the PbSe Nanocrystal Degradation. A JEOL 2100 electron microscope (Materials Science Division, Lawrence Berkeley National Laboratory) equipped with an environmental cell sample stage (Hummingbird Scientific) was used for in situ observation of the nanocrystals transformation upon air exposure under the electron beam. The environmental cells are made of two 4 mm^2 silicon chips with a 50 nm thick silicon nitride membrane window on each chip. The bottom chip has a 250–500 nm thick silicon dioxide spacer to allow air flow between the top and the bottom chip. This is a general setup for both liquid and gas flow. In our experiments, there is no flowing liquid or gas in the system. Instead, static gas exposure is used. First, 2 μL of 0.25 mg/mL oleate-capped nanocrystals dispersed in hexane was drop-casted on a silicon nitride viewing window (bottom chip) and dried to form a hexagonal close-packed nanocrystal monolayer. Then, the environmental cell was assembled by placing the top chip on the bottom chip and connecting the cell with the tubing. The inlet and outlet tubes were sealed by parafilm for some experiments and left open for other experiments. The above procedure was completed in the glovebox. During TEM imaging, with the end of the connecting tubes in air, a trace amount of air can diffuse through the parafilm into the tube and react with the sample. Therefore, two distinct scenarios for the nanocrystals with different degrees of air exposure were created by simply sealing the tube with parafilm or leaving it open. This is a simple qualitative but highly effective approach to varying the air exposure. In addition, we also used the conventional sample holder without connecting the tubes to image the nanocrystals, which completely eliminated oxygen exposure. The in situ experimental setup is shown in Figure 1.

The in situ study of PbSe nanocrystals in pure O$_2$ environment was performed using a FEI Titan 80-300 environmental transmission electron microscope (ETEM) operated at 300 kV. The sample was prepared by drop-casting 2 μL of 0.25 mg/mL PbSe suspension on a silicon nitride membrane.

We carried out ex situ experiments, including O$_2$ plasma treatment and thermal heating of nanocrystals under different vacuum conditions. TEM samples were prepared by drop-casting 4 μL of 0.25 mg/mL PbSe suspension on TEM carbon grids. The PbSe nanocrystals before and after the heating experiments were imaged using high-resolution TEM (HRTEM), high-angle annular dark-field scanning transmission electron microscopy (HAADF-STEM), and energy dispersive X-ray spectroscopy (EDS) with the aberration corrected electron microscopes (TEAM 1 and ThemIS) operated at 300 kV at the National Center for Electron Microscopy of Lawrence Berkeley National Laboratory. The O$_2$ plasma treatment was conducted on Fischione 1020 Plasma Cleaner.

■ RESULTS AND DISCUSSION

We study PbSe nanocrystal degradation under different degrees of air exposure in situ using the experimental setup shown in Figure 1 (see Experimental Section for more details). The nanocrystals undergo structural changes upon exposure to air inside the microscope. We use a low electron dose rate (<10 e$^-$ Å^{-2} s^{-1}) for in situ TEM imaging. Sequential TEM images of nanocrystals with full and partial air exposure are shown in Figure 2a,b (also see Movies S1 and S2). Under full
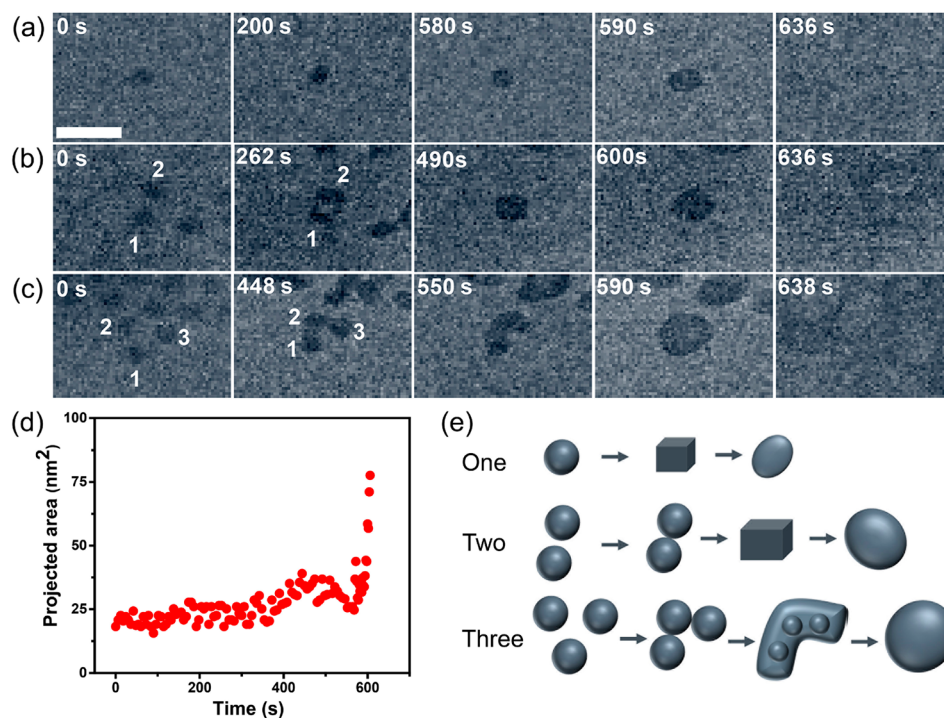
Figure 3. Morphology changes of a few selected PbSe nanocrystals when partially exposed to air. Sequential TEM images showing the morphology changes of (a) single, (b) two, and (c) three PbSe nanocrystals when partially exposed to air. (d) The projected area of the selected nanocrystals versus time shown in (a). (e) Schematics highlight the morphological evolution of PbSe nanocrystals observed in (a)−(c). All PbSe nanocrystals eventually form thin films by solid-state fusion. Scale bar: 20 nm.

air exposure, the PbSe nanocrystal superlattices undergo distinct structural modifications. First, the nanocrystals are mobilized on the membrane, breaking the symmetry of the original hexagonal superlattices. Second, nanocrystals fuse together into aggregates with irregular shape. Consequently, the nanocrystal size distribution becomes nonuniform. Third, there are drastic morphology changes of nanocrystals through solid-state fusion, suggesting that ligands have been removed from the nanocrystal surface by beam exposure in air. We propose that electron beam irradiation can introduce damages to the ligands and displacements of the ligands from nanocrystal surface.[40] The oxidative species generated by electron beam radiolysis of air (containing O_2 and H_2O)[41] promote ligand removal and surface oxidation of the nanocrystals. After ligands are displaced, the nanocrystals spread out and merge together. It is noted that, during the degradation process, the nanocrystals at the outer layer or edges of the hexagonal pattern change more dramatically compared with those nanocrystals inside the superlattice with six neighboring nanocrystals (Movie S1).

The morphology changes of nanocrystals are slower when nanocrystals are partially exposed to air compared to those that are fully exposed to air (Figure 2b; Movies S2 and S4). No obvious changes can be observed within the first 8−10 min under the same electron beam current density. After ~10 min (i.e., at 608 s), some nanocrystals start to get close to each other and they eventually coalesce to form large nanocrystals (Figure 2b). For both cases with different degrees of air exposure, nanocrystals follow the same trend of structural modification as shown in the schematic in Figure 2c. We trace the number of individual nanocrystals in each frame during degradation in both cases (Figure 2d; Movies S3 and S4). Nanocrystals undergo rapid agglomeration, leading to a single

irregular domain of mass in less than 60 s under full air exposure (Figure 2a). In contrast, the same process extends more than 10 min under partial air exposure, suggesting PbSe nanocrystals are much more stable under partial exposure to air.

We also trace the morphology evolution of individual PbSe nanocrystals in air. Figure 3 shows the structural evolution of a monomer, dimer, and trimer in the partial air-exposure condition (also see Movie S5). The monomer (Figure 3a) morphed after ~580 s from the initial sphere into a cuboid nanocrystal intermediate. The cuboid intermediates are commonly observed in many other nanocrystal degradation processes (Figure S1). In the next ~10 s, the projected area of the nanocrystal increases and the nanocrystal becomes more round, suggesting that the nanocrystal flattens. Subsequently, it transforms into an irregular domain. We measured the projected area of the monomer as a function of time (Figure 3d and Figure S1). No obvious changes are observed during the first ~500 s. Then, a cuboid intermediate is formed, after which a large increase in the projected area occurs. In the end (after ~600 s), the nanocrystal spreads to form a thin film. We consider that the degradation of PbSe nanocrystals begins with the removal of oleate ligands on the nanocrystals surface. Without ligand passivation, the nanocrystals change shape easily. Figure 3b shows the structural evolution of two nanocrystals under partial exposure to air. First, the two nanocrystals coalesce and form a dimer. Then, the dimer transforms into a spherical nanocrystal, and the subsequent changes of the nanocrystal are similar to the above single nanocrystal structural evolution as shown in Figure 3a. Figure 3c shows the evolution of three nanocrystals. They merge together to form a much bigger nanocrystal.

Although the observed degradation of PbSe nanocrystals is activated by the electron beam, the electron beam itself does not introduce morphological or structural changes of nanocrystals without introducing air into the system. We find that nanocrystals are quite stable for an extended period of time under electron beam in vacuum (see Figure S2 and Movie S6). In the air-free condition, nanocrystals do not show obvious changes after 444 s irradiation under a much higher electron beam dose rate ($\sim$1200 e$^-$ Å^{-2} s^{-1}). The morphology of individual nanocrystals and the center-to-center distance between nanocrystals within the hexagonal superlattices are maintained the same (Figure S2).

We characterize the PbSe nanocrystals after they are partially exposed to air under beam irradiation. Under the same air exposure, the morphology changes of PbSe nanocrystals are strongly dependent on the electron beam dose. As shown in Figure 4a, PbSe nanocrystals are subjected to nonuniform
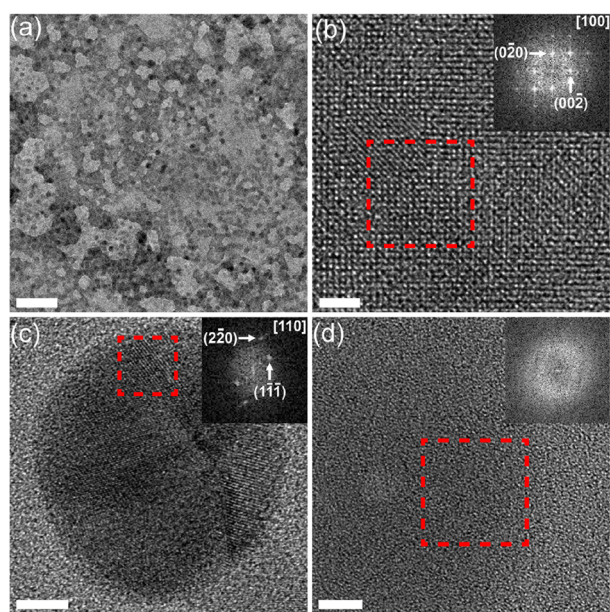

Figure 4. Characterization of PbSe nanocrystals after partial exposure to air under electron beam irradiation inside an environmental cell. Three types of products are found including PbSe thin film domains, pure Pb nanocrystals, and amorphous thin films. (a) Low magnification TEM image of PbSe nanocrystals with different morphological changes. (b) High resolution TEM image showing a region with PbSe thin film. (c) High resolution TEM image indicating a pure Pb nanocrystal. (d) Amorphous thin film. The insets in (b)−(d) are the corresponding FFT patterns of the selected areas. Scale bar for (a) is 50 nm; scale bar for (b) is 2 nm; and scale bars for (c) and (d) are 5 nm.

electron beam irradiation. The area (the upper right corner) with stronger electron beam irradiation shows that PbSe nanocrystals have turned into thin film domains, while the original PbSe nanocrystals are visible in areas with less electron beam exposure. Overall, three types of products are found during the nanocrystal structural evolution, including PbSe thin films (Figure 4b), pure Pb nanocrystals (Figure 4c), and amorphous thin film domains (Figure 4c). The formation of PbSe thin films results from the solid-state fusion of PbSe nanocrystals after coalescence (Movie S1). However, further study is needed in order to understand the formation mechanisms of pure Pb nanocrystals and the amorphous thin

films. We hypothesized that the degradation of PbSe nanocrystals is through their reaction with oxygen under the electron beam.

As control experiments, we study PbSe nanocrystals exposed to 1 mbar O_2 atmosphere for 368 s in a commercial environmental TEM (Movie S7 and Figure 5). Figure 5a
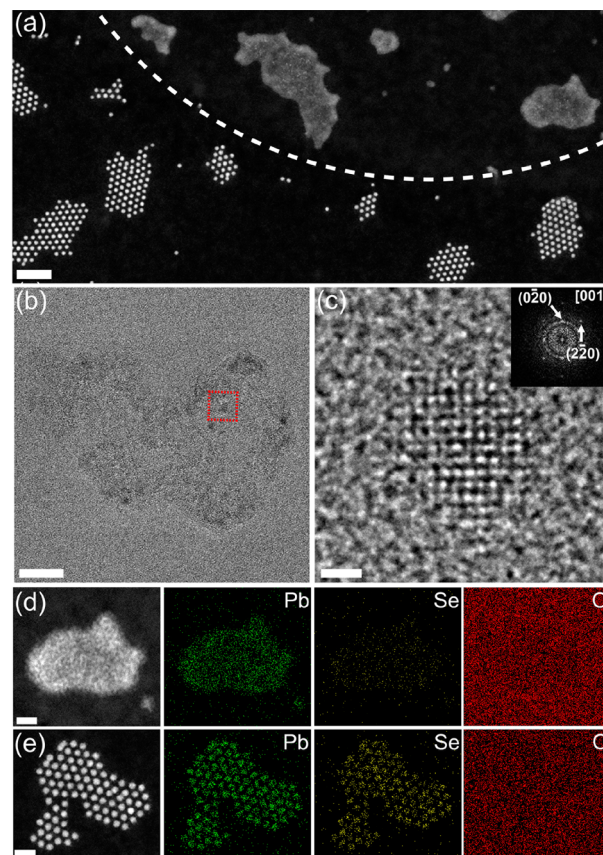

Figure 5. Characterization of PbSe nanocrystals after exposure to 1 mbar O_2 gas under electron irradiation in a commercial environmental TEM. (a) HAADF-STEM image of the nanocrystals after O_2 was introduced. The upper right corner area was irradiated under a dose rate of 50 e$^-$ Å^{-2} s^{-1}, and the rest area was not directly exposed to the electron beam. (b) TEM image of an irregular domain from the area after electron beam irradiation. (c) An enlarged area in (b) shows a remaining PbSe nanocrystal within the amorphous structure. The inset is the corresponding FFT pattern. (d) HAADF-STEM and EDS elemental maps of an irregular domain showing a Pb-rich phase. (e) HAADF-STEM and EDS elemental maps of an area without electron beam irradiation after introducing O_2. The original PbSe nanocrystals and the superlattice remain intact. Scale bar for (a) is 50 nm; scale bar for (b), (d), and (e) is 20 nm; and scale bar for (c) is 1 nm.

shows that all of the nanocrystals under electron beam irradiation have merged together to form irregular thin film domains, while in the region without electron radiation, the nanocrystals maintain the original hexagonal packing. The high resolution images of thin film domains (Figure 5b,c) show small PbSe nanocrystals within an amorphous structure (also see Figure S3). The STEM-EDS maps (Figure 5d) show that irregular domains are a Pb-rich phase. PbSe nanocrystals after air exposure without electron beam irradiation show the uniform distribution of Pb and Se within the nanocrystals (Figure 5e). When we increase the O_2 partial pressure from 1 mbar to 2 mbar, the PbSe nanocrystal degradation becomes

faster (Movie S7 and Movie S8). For instance, under 1 mbar of O_2, it takes 368 s for the hexagonal arrays of PbSe nanocrystals to turn into a thin film domain, while the reaction time is shortened to 236 s under 2 mbar. These results demonstrate that the exposure to oxygen under electron beam irradiation is responsible for the observed structural evolution of PbSe nanocrystals.

To illustrate the effects of water on the degradation mechanism of nanocrystals, we did additional in situ experiments using a self-contained liquid cell. PbSe nanocrystals are drop-casted on the membrane of a liquid cell, and 0.5 μL of deionized water is loaded into the liquid cell. PbSe nanocrystals in water experience degradation under an electron beam. Our observation reveals that the hexagonal packed arrays of PbSe nanocrystals first become a disordered structure (particles get close to each other) and subsequently the nanocrystals are dissolved under beam irradiation (Figures S4 and 5 and Movie S9). These results illustrate that water may accelerate the degradation of PbSe nanocrystals, which may arise from reactive species being generated by electrolysis of water under the electron beam.[42,43]

The reactive species promote the destruction and removal of the oleate ligands from the surface of nanocrystals (Figure 6a). We propose two routes of surface oxidation based on the surface facets with different ligands coverage. First, oxygen may directly adsorb on the (100) and (110) facets due to the sparse surface ligands (Figure 6b). The oxidation of the (111) facet is induced by the displacement of ligands (Figure 6c). Without surface ligands, the nanocrystal surfaces are unstable and surface diffusion of Pb and Se is activated. Consequently, coalescence and drastic morphology changes are observed, which lead to the formation of PbSe thin films. After that, Se is oxidized and evaporated from the PbSe nanocrystals, resulting an amorphous Pb rich phase (Figure 6d).

We further explore degradation of PbSe nanocrystals when they react with oxygen without electron beam irradiation. We first characterize PbSe nanocrystals on a carbon TEM grid after O_2 plasma treatment (a gas mixture of 25% oxygen and 75% argon for 30 s). We consider that the oxygen species generated in the plasma are highly reactive, which can effectively cause surface oxidation and ligand removal similar to the process under electron beam irradiation in air. The results show that the internanocrystal spacing is significantly reduced after O_2 plasma treatment (Figure 7). The average center-to-center
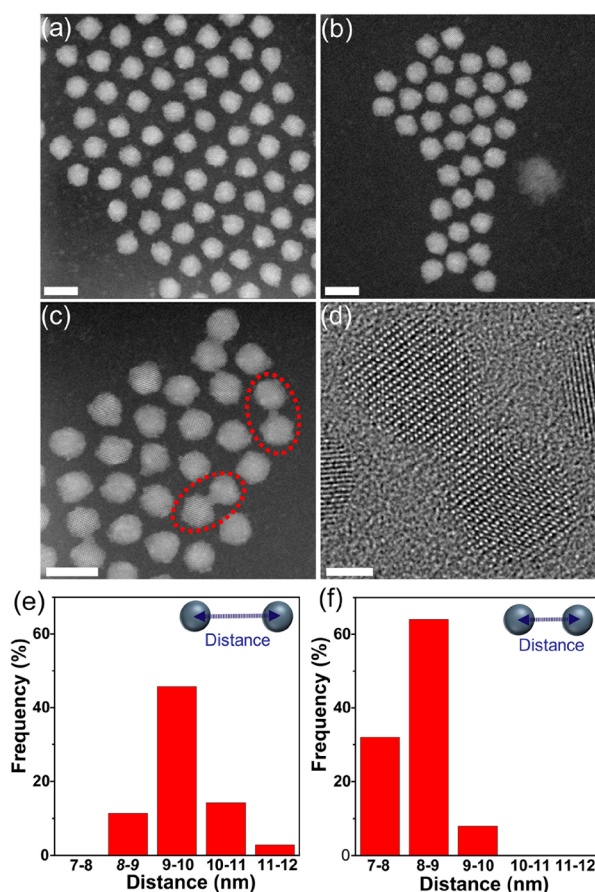
Figure 7. Effects of O_2 plasma treatment on PbSe nanocrystals. (a and b) HAADF-STEM images of PbSe nanocrystals before and after O_2 plasma treatment. (c and d) High resolution STEM and TEM images of PbSe nanocrystals with necking formation. (e and f) Statistical measurements of the distance between PbSe nanocrystals before and after O_2 plasma treatment corresponding to (a) and (b). Scale bars for images in (a), (b), and (c) are 10 nm. Scale bar for (d) is 2 nm.
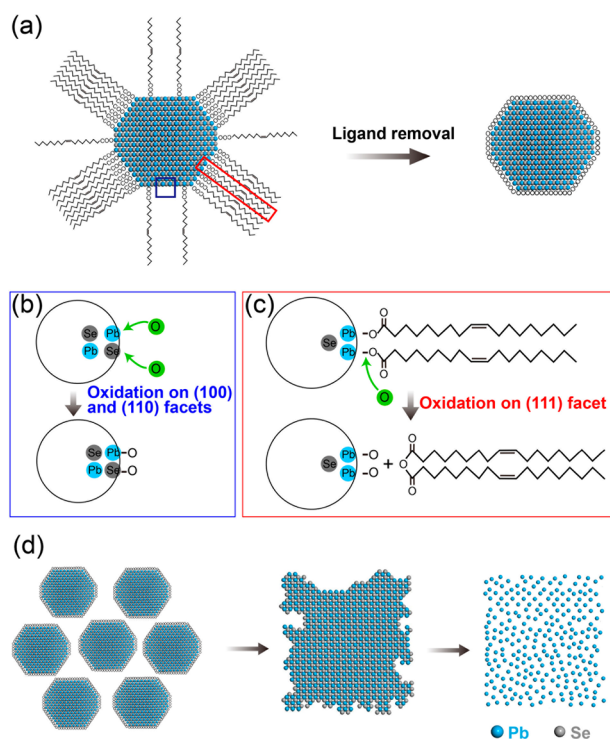

Figure 6. Proposed degradation mechanisms of PbSe nanocrystals when they are exposed to air under electron beam radiation. (a) Schematic of ligand removal due to surface oxidation. Fragmentations of the ligands under beam irradiation are neglected. (b) Oxygen chemi-adsorption on (100) and (110) facets. (c) Oxygen chemi-adsorption on (111) facet to form an oxide layer after the displacement of ligands. (d) After ligands removal, PbSe nanocrystals are merged together to form thin films, and they transform into a Pb-rich phase due to the oxidation and evaporation of Se.

distance between nanocrystals reduces from 9.1 to 8.3 nm. Some nanocrystals are even connected, forming a neck between two nanocrystals. We also compare the structure and morphology changes of PbSe nanocrystals with different degrees of air exposure under thermal heating (Figure 8). PbSe nanocrystals on TEM carbon grids were baked at 100 °C in a
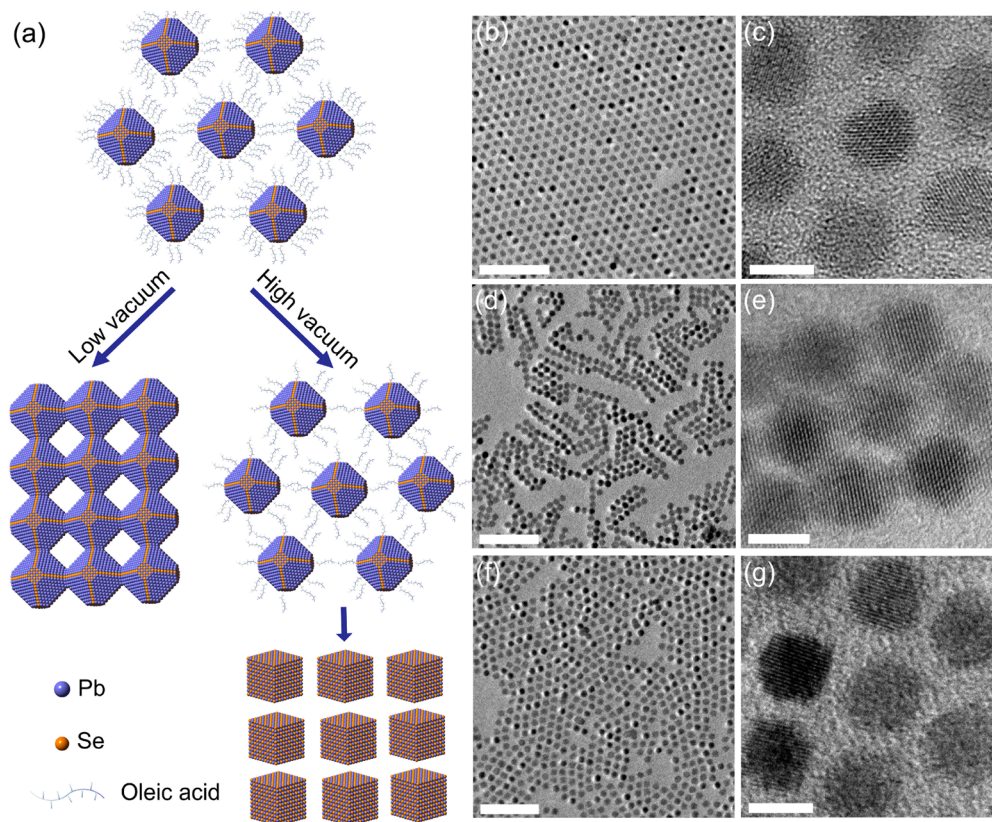
Figure 8. Ex situ experiments of heating PbSe nanocrystals at 100 °C in different vacuum conditions. (a) Schematic showing the structural evolution of PbSe nanocrystal superlattices during heating in different vacuum conditions. (b) Low and (c) and high magnification TEM images of monolayer films of PbSe superlattices after baking at 100 °C for 30 min in a high vacuum of 10^{-6} mbar. (d) Low and (e) high magnification TEM images of monolayer films of PbSe superlattices after baking at 100 °C for 30 min in a low vacuum of 1 mbar. (f) Low and (g) high magnification images of monolayer films of PbSe superlattices after baking at 100 °C for 12 h in a high vacuum of 10^{-6} mbar. Scale bars for images (b), (d), and (f) are 50 nm; scale bars for images (c), (e), and (g) are 5 nm.

heating station with controllable vacuum levels, for example, under low vacuum (1 mbar) and high vacuum (10^{-6} mbar) for 30 min and for 12 h. These experiments help us to understand PbSe nanocrystal degradation kinetics in air without electron beam effects.

Under high vacuum (10^{-6} mbar), the PbSe nanocrystal superlattices are well maintained after 30 min at 100 °C (Figure 8b). The high-resolution TEM image of nanocrystals shows that the neighboring nanocrystals are in different crystallographic orientations (Figure 8c). Baking at 100 °C in low vacuum (1 mbar) for 30 min results in epitaxially fused nanocrystals (Figure 8d,e). After longer time baking at 100 °C in low vacuum (1 mbar), more PbSe nanocrystals are connected to form a large scale pseudohexagonal pattern (Figure S6). For comparison, PbSe nanocrystals were also annealed at 100 °C in high vacuum (10^{-6} mbar) for 12 h. The results show that PbSe nanocrystals are not connected with each other. However, individual nanocrystals become cubes, and the interparticle distances are reduced (Figure 8f,g). According to previous studies, the nonpolar (100) facet is the most stable facet compared to the (110), (111), or other facets if ligands are completely removed.[44,45] We consider that variations in the pathways of PbSe nanocrystal structural transformations (Figure 8a) are determined by different oxygen partial pressure under different vacuum conditions. This is because when nanocrystals are exposed to oxygen, the surface atoms are susceptible to be oxidized, causing the loss of the oleic ligands.[15]

Further degradation of PbSe nanocrystals in air is accomplished by baking PbSe nanocrystals on a carbon TEM grid at 200 °C. After baking for 5 min, PbSe nanocrystals are connected by oriented attachment (Figure S7), which is similar to the results of heating in low vacuum for a much longer time (i.e., 30 min under 1 mbar in Figure 8d,e). After baking at 200 °C for 2 h, PbSe nanocrystals are transformed into nanorods (Figure 9a). The high-resolution TEM image of a connected PbSe nanorod shows that clusters of the PbSe crystal lattice remains in the core while most of the nanocrystal is amorphous (see the inset FFT; Figure 9b).

After baking for 12 h in air, most of the nanorods maintain their shape (Figure 9c), but all the nanorods become amorphous (Figure 9d; also see Figure S8). EDS elemental maps show that the amorphous nanorods are Pb−Se−oxide (Figure 9e). Further quantification of the EDS spectra indicates that the atomic ratio of Pb:Se:O is close to 1:1:3 (Figure S9).

■ CONCLUSION

Using in situ TEM with an environmental cell connected to air, we have studied the structural and morphological evolution of PbSe nanocrystals in air under electron beam irradiation. We find that the nanocrystal degradation process involves ligand dissociation and removal, shape evolution of individual nanocrystals with cuboid intermediates, coalescence between nanocrystals, formation of PbSe thin films through drastic
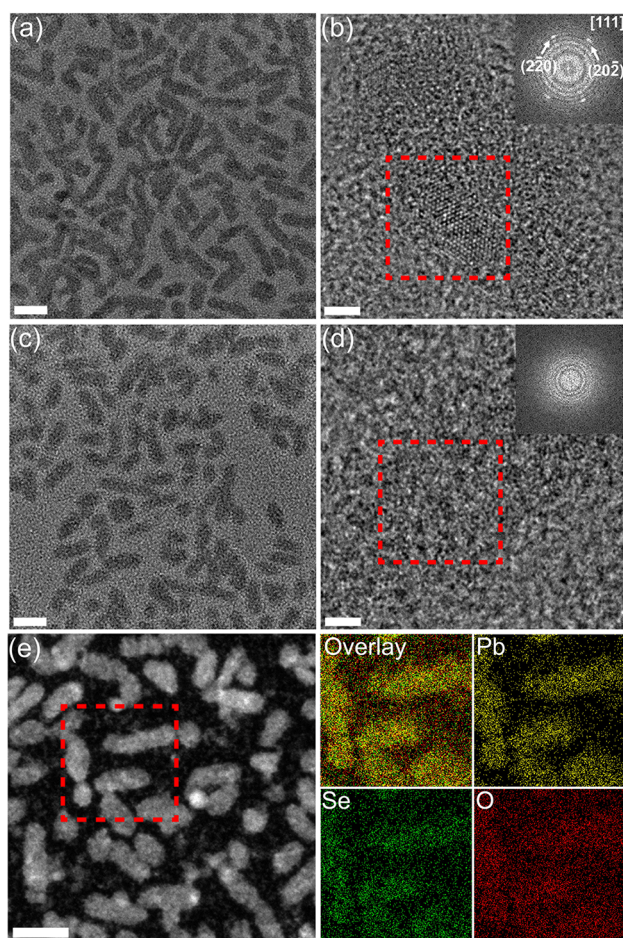
Figure 9. PbSe nanocrystals after baking at 200 °C in air. (a) Low and (b) high magnification TEM images of PbSe nanocrystals after baking in air at 200 °C for 2 h. The inset is the FFT pattern of the selected area in (b) showing the existence of small PbSe nanocrystals. (c) Low and (d) high magnification TEM images of PbSe nanocrystals after baking in air at 200 °C for 12 h. The inset is the FFT pattern of the selected area in (d) indicating the amorphous structure. (e) STEM image and EDS elemental maps of PbSe nanocrystals after baking in air at 200 °C for 12 h. Scale bars for images (a), (c), and (e) are 20 nm. Scale bars for images (b) and (d) are 2 nm.

solid-state fusion, and phase transformations from PbSe thin films to an amorphous Pb rich phase or eventually pure Pb. We have also conducted a series of in situ and ex situ experiments as complementary studies, including in situ environmental TEM study of PbSe nanocrystals exposed to pure oxygen, in situ TEM of PbSe nanocrystals in water using a liquid cell, and ex situ experiments of PbSe nanocrystals after O_2 plasma treatment or thermal heating with controlled air exposure. These complementary experiments allow for elucidating the role of oxygen, water, and electron beam in the observed nanocrystal degradation. These various in situ and ex situ experimental results indicate that PbSe nanocrystal degradation in air is initiated by the dissociation and removal of ligands from the PbSe nanocrystal surface when reacting with oxygen. Based on our studies in this work, we highlight these two points for the applications of PbSe nanocrystals: (i) Surface chemistry of nanocrystals greatly affects the stability of nanocrystals. Surface passivation of individual nanocrystals could help to improve air stability of the devices. (ii) In addition to individual nanocrystals, strategies that prevent the

nanocrystal superlattice from degradation is necessary to improve the lifetime of the devices. Lastly, this work highlights the versatility of the environmental cell for in situ TEM studies of the fading mechanism of PbSe or other nanocrystal-based devices. In addition, our in situ environmental cell setup may be applied to the study of many other air-sensitive materials (e.g., metal organic frameworks, perovskite materials, battery materials, etc.) including their responses to the exposure of air, moisture, or other reactive gases.

■ ASSOCIATED CONTENT

ⓢ Supporting Information

In situ TEM Movie S1−S9 (AVI) The Supporting Information is available free of charge on the ACS Publications website at DOI: 10.1021/acs.chemmater.8b04052.

> Morphology changes of single nanocrystals when partially exposed to air; TEM images and sized distribution of PbSe nanocrystals in vacuum under beam irradiation; TEM images of nanocrystals after introducing 1 mbar O_2; sequential TEM images of nanocrystals in water; and TEM images, SAED, and EDS maps of nanocrystals being heated under different conditions (PDF)

In situ TEM Movie S1 (AVI)
In situ TEM Movie S2 (AVI)
In situ TEM Movie S3 (AVI)
In situ TEM Movie S4 (AVI)
In situ TEM Movie S5 (AVI)
In situ TEM Movie S6 (AVI)
In situ TEM Movie S7 (AVI)
In situ TEM Movie S8 (AVI)
In situ TEM Movie S9 (AVI)

■ AUTHOR INFORMATION

Corresponding Authors
*E-mail: hgliao@xmu.edu.cn (H.-G.L.).
*E-mail: hmzheng@lbl.gov (H.Z.).
ORCID ⓘ
Xinxing Peng: 0000-0002-7077-8454
Zu-Wei Yin: 0000-0002-0728-1154
Shi-Gang Sun: 0000-0003-2327-4090
Haimei Zheng: 0000-0003-3813-4170
Notes
The authors declare no competing financial interest.

■ ACKNOWLEDGMENTS

■ REFERENCES

(1) Sargent, E. H. Colloidal quantum dot solar cells. *Nat. Photonics* **2012**, *6*, 133−135.

(2) Caruge, J.; Halpert, J. E.; Wood, V.; Bulović, V.; Bawendi, M. Colloidal quantum-dot light-emitting diodes with metal-oxide charge transport layers. *Nat. Photonics* **2008**, *2*, 247−250.

(3) Talapin, D. V.; Murray, C. B. PbSe nanocrystal solids for n- and p-channel thin film field-effect transistors. *Science* **2005**, *310*, 86−89.

(4) Boneschanscher, M. P.; Evers, W. H.; Geuchies, J. J.; Altantzis, T.; Goris, B.; Rabouw, F. T.; van Rossum, S. A.; van der Zant, H. S.; Siebbeles, L. D.; Van Tendeloo, G.; Swart, I.; Hilhorst, J.; Petukhov, A. V.; Bals, S.; Vanmaekelbergh, D. Long-range orientation and atomic attachment of nanocrystals in 2D honeycomb superlattices. *Science* **2014**, *344*, 1377−1380.

(5) Shevchenko, E. V.; Talapin, D. V.; Kotov, N. A.; O'Brien, S.; Murray, C. B. Structural diversity in binary nanoparticle superlattices. *Nature* **2006**, *439*, 55−59.

(6) Dong, A.; Chen, J.; Vora, P. M.; Kikkawa, J. M.; Murray, C. B. Binary nanocrystal superlattice membranes self-assembled at the liquid-air interface. *Nature* **2010**, *466*, 474−477.

(7) Evers, W. H.; Goris, B.; Bals, S.; Casavola, M.; de Graaf, J.; van Roij, R.; Dijkstra, M.; Vanmaekelbergh, D. Low-dimensional semiconductor superlattices formed by geometric control over nanocrystal attachment. *Nano Lett.* **2013**, *13*, 2317−2323.

(8) Whitham, K.; Yang, J.; Savitzky, B. H.; Kourkoutis, L. F.; Wise, F.; Hanrath, T. Charge transport and localization in atomically coherent quantum dot solids. *Nat. Mater.* **2016**, *15* (5), 557−563.

(9) Whitham, K.; Hanrath, T. Formation of Epitaxially Connected Quantum Dot Solids: Nucleation and Coherent Phase Transition. *J. Phys. Chem. Lett.* **2017**, *8*, 2623−2628.

(10) Geuchies, J. J.; van Overbeek, C.; Evers, W. H.; Goris, B.; de Backer, A.; Gantapara, A. P.; Rabouw, F. T.; Hilhorst, J.; Peters, J. L.; Konovalov, O.; Petukhov, A. V.; Dijkstra, M.; Siebbeles, L. D.; van Aert, S.; Bals, S.; Vanmaekelbergh, D. *In situ* study of the formation mechanism of two-dimensional superlattices from PbSe nanocrystals. *Nat. Mater.* **2016**, *15*, 1248−1254.

(11) Baumgardner, W. J.; Whitham, K.; Hanrath, T. Confined-but-connected quantum solids via controlled ligand displacement. *Nano Lett.* **2013**, *13*, 3225−3231.

(12) Xu, L.; Liang, H.-W.; Yang, Y.; Yu, S.-H. Stability and Reactivity: Positive and Negative Aspects for Nanoparticle Processing. *Chem. Rev.* **2018**, *118*, 3209−3250.

(13) Luther, J. M.; Law, M.; Song, Q.; Perkins, C. L.; Beard, M. C.; Nozik, A. J. Structural, optical, and electrical properties of self-assembled films of PbSe nanocrystals treated with 1, 2-ethanedithiol. *ACS Nano* **2008**, *2*, 271−280.

(14) Cho, K.-S.; Talapin, D. V.; Gaschler, W.; Murray, C. B. Designing PbSe nanowires and nanorings through oriented attachment of nanoparticles. *J. Am. Chem. Soc.* **2005**, *127*, 7140−7147.

(15) Moreels, I.; Fritzinger, B.; Martins, J. C.; Hens, Z. Surface chemistry of colloidal PbSe nanocrystals. *J. Am. Chem. Soc.* **2008**, *130*, 15081−15086.

(16) Argeri, M.; Fraccarollo, A.; Grassi, F.; Marchese, L.; Cossi, M. Density functional theory modeling of PbSe nanoclusters: effect of surface passivation on shape and composition. *J. Phys. Chem. C* **2011**, *115*, 11382−11389.

(17) Woo, J. Y.; Ko, J. H.; Song, J. H.; Kim, K.; Choi, H.; Kim, Y. H.; Lee, D. C.; Jeong, S. Ultrastable PbSe nanocrystal quantum dots via *in situ* formation of atomically thin halide adlayers on PbSe(100). *J. Am. Chem. Soc.* **2014**, *136*, 8883−8886.

(18) Law, M.; Luther, J. M.; Song, Q.; Hughes, B. K.; Perkins, C. L.; Nozik, A. J. Structural, optical, and electrical properties of PbSe nanocrystal solids treated thermally or with simple amines. *J. Am. Chem. Soc.* **2008**, *130*, 5974−5985.

(19) Dai, Q.; Wang, Y.; Zhang, Y.; Li, X.; Li, R.; Zou, B.; Seo, J.; Wang, Y.; Liu, M.; Yu, W. W. Stability study of PbSe semiconductor nanocrystals over concentration, size, atmosphere, and light exposure. *Langmuir* **2009**, *25*, 12320−12324.

(20) Gautier, C.; Cambon-Muller, M.; Averous, M. Study of PbSe layer oxidation and oxide dissolution. *Appl. Surf. Sci.* **1999**, *141*, 157−163.

(21) Tomaev, V. V.; Makarov, L. L.; Tikhonov, P. A.; Solomennikov, A. A. Oxidation kinetics of lead selenide. *Glass Phys. Chem.* **2004**, *30* (4), 349−355.

(22) Sykora, M.; Koposov, A. Y.; McGuire, J. A.; Schulze, R. K.; Tretiak, O.; Pietryga, J. M.; Klimov, V. I. Effect of air exposure on surface properties, electronic structure, and carrier relaxation in PbSe nanocrystals. *ACS Nano* **2010**, *4*, 2021−2034.

(23) Goodfellow, B. W.; Patel, R. N.; Panthani, M. G.; Smilgies, D. M.; Korgel, B. A. Melting and Sintering of a Body-Centered Cubic Superlattice of PbSe Nanocrystals Followed by Small Angle X-ray Scattering. *J. Phys. Chem. C* **2011**, *115*, 6397−6404.

(24) Shi, W.; Eijt, S. W. H.; Suchand Sandeep, C. S.; Siebbeles, L. D. A.; Houtepen, A. J.; Kinge, S.; Brück, E.; Barbiellini, B.; Bansil, A. Ligand-surface interactions and surface oxidation of colloidal PbSe quantum dots revealed by thin-film positron annihilation methods. *Appl. Phys. Lett.* **2016**, *108*, 081602.

(25) Lian, L.; Xia, Y.; Zhang, C.; Xu, B.; Yang, L.; Liu, H.; Zhang, D.; Wang, K.; Gao, J.; Zhang, J. *In Situ* Tuning the Reactivity of Selenium Precursor to Synthesize Wide Range Size, Ultralarge-Scale, and Ultrastable PbSe Quantum Dots. *Chem. Mater.* **2018**, *30*, 982−989.

(26) Zhang, Z.; Chen, Z.; Yuan, L.; Chen, W.; Yang, J.; Wang, B.; Wen, X.; Zhang, J.; Hu, L.; Stride, J. A.; Conibeer, G. J.; Patterson, R. J.; Huang, S. A New Passivation Route Leading to Over 8% Efficient PbSe Quantum-Dot Solar Cells via Direct Ion Exchange with Perovskite Nanocrystals. *Adv. Mater.* **2017**, *29*, 1703214−1703222.

(27) Wang, Y.; Lu, K.; Han, L.; Liu, Z.; Shi, G.; Fang, H.; Chen, S.; Wu, T.; Yang, F.; Gu, M.; et al. In Situ Passivation for Efficient PbS Quantum Dot Solar Cells by Precursor Engineering. *Adv. Mater.* **2018**, *30*, 1704871−1704819.

(28) Pietryga, J. M.; Werder, D. J.; Williams, D. J.; Casson, J. L.; Schaller, R. D.; Klimov, V. I.; Hollingsworth, J. A. Utilizing the lability of lead selenide to produce heterostructured nanocrystals with bright, stable infrared emission. *J. Am. Chem. Soc.* **2008**, *130*, 4879−4885.

(29) Liu, Y.; Gibbs, M.; Perkins, C. L.; Tolentino, J.; Zarghami, M. H.; Bustamante, J., Jr; Law, M. Robust, functional nanocrystal solids by infilling with atomic layer deposition. *Nano Lett.* **2011**, *11*, 5349−5355.

(30) Zhang, X.; Meng, J.; Zhu, B.; Yu, J.; Zou, S.; Zhang, Z.; Gao, Y.; Wang, Y. *In situ* TEM studies of the shape evolution of Pd nanocrystals under oxygen and hydrogen environments at atmospheric pressure. *Chem. Commun.* **2017**, *53*, 13213−13216.

(31) Xin, H. L.; Niu, K.; Alsem, D. H.; Zheng, H. *In situ* TEM study of catalytic nanoparticle reactions in atmospheric pressure gas environment. *Microsc. Microanal.* **2013**, *19*, 1558−1568.

(32) Nielsen, M. H.; Aloni, S.; De Yoreo, J. J. *In situ* TEM imaging of CaCO$_3$ nucleation reveals coexistence of direct and indirect pathways. *Science* **2014**, *345*, 1158−1162.

(33) Avanesian, T.; Dai, S.; Kale, M. J.; Graham, G. W.; Pan, X.; Christopher, P. Quantitative and atomic-scale view of CO-induced Pt nanoparticle surface reconstruction at saturation coverage via DFT calculations coupled with *in situ* TEM and IR. *J. Am. Chem. Soc.* **2017**, *139*, 4551−4558.

(34) Zheng, H.; Smith, R. K.; Jun, Y.-w.; Kisielowski, C.; Dahmen, U.; Alivisatos, A. P. Observation of single colloidal platinum nanocrystal growth trajectories. *Science* **2009**, *324*, 1309−1312.

(35) Evans, J. E.; Jungjohann, K. L.; Browning, N. D.; Arslan, I. Controlled growth of nanoparticles from solution with *in situ* liquid transmission electron microscopy. *Nano Lett.* **2011**, *11*, 2809−2813.

(36) Liao, H.-G.; Zherebetskyy, D.; Xin, H.; Czarnik, C.; Ercius, P.; Elmlund, H.; Pan, M.; Wang, L.-W.; Zheng, H. Facet development during platinum nanocube growth. *Science* **2014**, *345*, 916−919.

(37) Ross, F. M. Opportunities and challenges in liquid cell electron microscopy. *Science* **2015**, *350*, aaa9886.

(38) Liang, W. I.; Zhang, X.; Zan, Y.; Pan, M.; Czarnik, C.; Bustillo, K.; Xu, J.; Chu, Y. H.; Zheng, H. *In Situ* Study of Fe$_3$Pt-Fe$_2$O$_3$ Core-

Shell Nanoparticle Formation. *J. Am. Chem. Soc.* **2015**, *137*, 14850−14853.

(39) Zeng, Z.; Zheng, W.; Zheng, H. Visualization of Colloidal Nanocrystal Formation and Electrode-Electrolyte Interfaces in Liquids Using TEM. *Acc. Chem. Res.* **2017**, *50*, 1808−1817.

(40) Azcárate, J. C.; Fonticelli, M. H.; Zelaya, E. Radiation Damage Mechanisms of Monolayer-Protected Nanoparticles via TEM Analysis. *J. Phys. Chem. C* **2017**, *121*, 26108−26116.

(41) Willis, C.; Boyd, A. Excitation in the radiation chemistry of inorganic gases. Int. J. Raidat. *Int. J. Radiat. Phys. Chem.* **1976**, *8*, 71−111.

(42) Allen, A. O. *The radiation chemistry of water and aqueous solutions*; Van Nostrand: Princeton, NJ, 1961.

(43) Sehested, K.; Rasmussen, O. L.; Fricke, H. Rate constants of OH with HO_2, O_2^-, and $H_2O_2^+$ from hydrogen peroxide formation in pulse-irradiated oxygenated water. *J. Phys. Chem.* **1968**, *72*, 626−631.

(44) Fang, C.; van Huis, M. A.; Vanmaekelbergh, D.; Zandbergen, H. W. Energetics of polar and nonpolar facets of PbSe nanocrystals from theory and experiment. *ACS Nano* **2010**, *4*, 211−218.

(45) Schapotschnikow, P.; van Huis, M. A.; Zandbergen, H. W.; Vanmaekelbergh, D.; Vlugt, T. J. Morphological transformations and fusion of PbSe nanocrystals studied using atomistic simulations. *Nano Lett.* **2010**, *10*, 3966−3971.